Copyright © 2013 Tech Science Press CMES, vol.94, no.6, pp.459-483, 2013

FEM/Wideband FMBEM Coupling for Fluid-Structure Interaction Problem and 2D Acoustic Design Sensitivity Analysis

L.L. Chen[1], **H.B. Chen**[2] **and C.J. Zheng**[3]

Abstract: A coupling algorithm based on the finite element method and the wideband fast multipole boundary element method (FEM/wideband FMBEM) is proposed for the simulation of fluid-structure interaction and structural-acoustic sensitivity analysis using the direct differentiation method. The wideband fast multipole method (FMM) formed by combining the original FMM and the diagonal form FMM is used to accelerate the matrix-vector products in the boundary element analysis. The iterative solver GMRES is applied to accelerate the solution of the linear system of equations. The FEM/Wideband FMBEM algorithm makes it possible to predict the effects of arbitrarily shaped vibrating structures on the sound field numerically. Numerical examples are presented to demonstrate the validity and efficiency of the proposed algorithm.

Keywords: Fluid-structure interaction, FEM, Wideband FMBEM, Design sensitivity analysis, Direct differentiation method.

1 Introduction

Analysis of the acoustic radiation or scattering from elastic structure in heavy fluid is a classical problem of underwater acoustics. Analytical solutions to the acoustic fluid-structure interaction problems are only available when the structure has simple geometry with simple boundary conditions [Junger and Feit (1985)]. For more

[1] Department of Modern Mechanics, University of Science and Technology of China, CAS Key Laboratory of Mechanical Behavior and Design of Materials, Hefei 230027, Anhui, P.R.China. Email: chenllei@mail.ustc.edu.cn

[2] Corresponding Author. Department of Modern Mechanics, University of Science and Technology of China, CAS Key Laboratory of Mechanical Behavior and Design of Materials, Hefei 230027, Anhui, P.R.China. Phone:+86-0551-63600345. Fax:+86-0551-63606459. Email: hbchen@ustc.edu.cn

[3] Department of Modern Mechanics, University of Science and Technology of China, CAS Key Laboratory of Mechanical Behavior and Design of Materials, Hefei 230027, Anhui, P.R.China. Email: cjzheng@ustc.edu.cn

practical problems with complicated geometries, it is impossible to find analytical solutions, and thus necessary to create efficient numerical methods.

FEM has been widely used to the analysis of the dynamic behavior of structure, acoustic and fluid-structure interaction problems. However, the FEM has its limitations in modeling infinite domains. It is well-known that BEM has been widely used to solve acoustic problems, because it provides an excellent accuracy and easy mesh generation. In particular, for exterior acoustic problems, the Sommerfeld radiation condition at infinite is automatically satisfied. So, a suitable approach for the analysis of fluid-structure interaction problems is the coupled FEM/BEM [Everstine and Henderson (1990); Fritze, Marburg, and Hardtke (2005); Chen, Hofstetter, and Mang (1998)]. But the coupling analysis of structural-acoustic underwater based on FEM/Conventional BEM (CBEM) algorithm still represents the bottleneck of large computation cost, because the CBEM produces a dense and non-symmetrical coefficient matrix which induces $O(N^3)$ arithmetic operations to solve the system of equations directly, such as by using the Gauss elimination method. The fast multipole method(FMM) [Greengard and Rokhlin (1987); Coifman, Rokhlin, and Wandzura (1993); Song, Lu, and Chew (1997); Darve and P.Havé (2004); Rokhlin (1993); Shen and Liu (2007); Zheng, Chen, Matsumoto, and Takahashi (2012)] has been presented to accelerate the solution of the CBEM system of equations and to decrease the memory requirement. And the coupling algorithm based on FEM/fast multipole boundary element method (FEM/FMBEM) had been applied to solve the large scale fluid-structure interaction problems [Schneider (2008); Fischer and Gaul (2005)].

There are actually two FMM forms for Helmholtz equation. One is the original FMM and the other is the diagonal form. It is well known that both of them fail in some way outside their preferred frequency ranges. However wideband FMM formed by combining the original FMM and the diagonal form FMM can overcome the above problems [Cheng, Crutchfield, Gimbutas, Greengard, Ethridge, Huang, Rokhlin, Yarvin, and Zhao (2006); Gumerov and Duraiswami (2009); Wolf and Lele (2011); Zheng, Matsumoto, Takahashi, and Chen (2012)]. In this paper the coupling algorithm FEM/Wideband FMBEM is proposed to solve the large scale fluid-structure interaction problems.

Passive noise control by modification of structure geometry moves more and more into the field of vision for designers. This structural-acoustic optimization shows high potential in minimization of radiated noise especially for thin shell geometries [Kim and Dong (2006); Zheng, Matsumoto, Takahashi, and Chen (2011); Matsumoto, Yamada, Takahashi, Zheng, and Harada (2011); Zheng, Chen, Matsumoto, and Takahashi (2011); Chen, Zheng, and Chen (2013)]. Acoustic design sensitivity analysis can provide information on how the geometry change affects the acoustic performance of the given structure, so it is an important step of the acoustic design and optimization processes. But the sensitivity analysis of the structural-acoustic interaction based on FEM/Conventional BEM algorithm represents the bottleneck in computation efforts. In this paper, the coupling algorithm FEM/Wideband FMBEM is applied to the structural-acoustic sensitivity analysis based on direct differentiation method.

This work promotes the applications of coupling FEM/Wideband FMBEM in the fluid-structure interaction problems. The original FMM, diagonal form FMM and wideband FMM are presented in this paper. Examples of scattering from underwater cylindrical shell are presented to demonstrate the accuracy and efficiency of this method.

2 Structural-acoustic analysis

2.1 FEM modeling

It is assumed that a harmonic load with the excitation frequency ω is applied to the structure, the steady-state response of the structure can be calculated from the frequency-response analysis. The linear system of equations to compute the nodal displacements u is derived by

$$(\mathbf{K}+i\omega\mathbf{C}-\omega^2\mathbf{M})\mathbf{u}(\omega)=\mathbf{A}\mathbf{u}=\mathbf{f}, \tag{1}$$

where $i=\sqrt{-1}$, $\mathbf{M}$ the mass matrix, $\mathbf{K}$ the stiffness matrix, $\mathbf{C}$ the damping matrix and $\mathbf{u}$ the nodal displacement vector. Note that the steady-state response has the same frequency as the applied load but may have a different phase angle due to the existence of damping. If the applied load is not harmonic, Eq. 1 can still be applied by decomposing the time-dependent forces into the frequency domain. Taking into account the effect of the acoustic pressure at the structural surfaces, we apply an acoustic load $\mathbf{C_{sf}p}$ along with the structural load $\mathbf{f_s}$, and then the excitation can be expressed as:

$$\mathbf{f}=\mathbf{f_s}+\mathbf{C_{sf}p}, \tag{2}$$

where the coupling matrix $\mathbf{C_{sf}}$ transforms the degrees of freedom of the fluid to the structural degrees of freedom, and it can be expressed as:

$$\mathbf{C_{sf}}=\int_{\Gamma_{int}}\mathbf{N_s^T}\mathbf{n}\mathbf{N_f}d\Gamma_{int}, \tag{3}$$

where Γ_{int} denotes the interaction surface, $\mathbf{N_s}$ and $\mathbf{N_f}$ are the global interpolation functions for the structure and fluid domains, respectively, $\mathbf{n}$ is the surface normal vector. By substituting Eq. 2 into Eq. 1, we can obtain the following formula

$$\mathbf{u}=\mathbf{A}^{-1}\mathbf{f_s}+\mathbf{A}^{-1}\mathbf{C_{sf}p}. \tag{4}$$

2.2 BEM modeling

Consider the following Helmholtz equation governing a time-harmonic acoustic wave field:

$$\nabla^2 p(x) + k^2 p(x) = 0, \qquad \forall x \in \Omega, \tag{5}$$

where P is the acoustic pressure, $k = \omega/c$ the wave number, ω the angular frequency, and c the wave speed in the acoustic medium Ω. The boundary conditions can be expressed as

$$p(x) = \overline{p}(x) \qquad x \in S_p, \tag{6}$$

$$q(x) = \frac{\partial p(x)}{\partial n(x)} = i\rho\omega\overline{v}(x) \qquad x \in S_q, \tag{7}$$

$$p(x) = zv(x) \qquad x \in S_z, \tag{8}$$

where $n(x)$ denotes the outward unit normal vector to the boundary S at point x, ρ the medium density, $v(x)$ the normal velocity, z the acoustic impedance. The quantities with upper bars are assumed to be known functions prescribed on the boundary.

The Helmholtz equation can be reformulated into a boundary integral equation (BIE) defined on the structure boundary S as follows:

$$c(x)p(x) + \int_S F(x,y)p(y)\,\mathrm{d}S(y) = \int_S G(x,y)q(y)\,\mathrm{d}S(y) + p_i(x), \tag{9}$$

where the coefficient $c(x)$ is $1/2$ if S is smooth around the source point x, $p_i(x)$ the incident wave, $q(y)$ and $F(x,y)$ the normal derivatives of $p(y)$ and $G(x,y)$, y the field point, and $G(x,y)$ the Green's function. As for two dimensional acoustic wave problems, $G(x,y)$ is given as

$$G(x,y) = \frac{i}{4} H_0^{(1)}(kr). \tag{10}$$

On the other hand, the implementation of a single Helmholtz boundary integral equation may have the difficulty of nonuniqueness for exterior boundary-value problems. But Burton-Miller method which consists of a linear combination of the conventional boundary integral equation and its normal derivative equation can be applied to overcome the nonuniqueness problem efficiently [Burton and Miller (1971)].

If the boundary S is divided into N elements (e.g. using piecewise constant discretization in this study). Then, after collecting the equations for all collocation points (nodes) located at the centre of each element and expressing them in matrix forms, one can obtain the following system of linear algebraic equations

$$\mathbf{Hp} = \mathbf{Gq} + \mathbf{p_i}. \tag{11}$$

2.3 FEM/BEM modeling

The governing equations shown above are linked up via the continuity condition $\mathbf{q} = -i\omega\rho\mathbf{v}$ across the interaction surface. The normal velocity $\mathbf{v}$ can be expressed as a function of the displacement $\mathbf{u}$, as follows

$$\mathbf{v} = i\omega\mathbf{S^{-1}C_{fs}u}, \tag{12}$$

where $\mathbf{S} = \int_{\Gamma_{int}} \mathbf{N_f^T N_f} d\Gamma_{int}$ and $\mathbf{C_{fs}} = \mathbf{C_{sf}^T}$. By substituting Eq. 12 into Eq. 11, we can obtain the following formulation

$$\mathbf{Hp} = \omega^2\rho\mathbf{GS^{-1}C_{fs}u} + \mathbf{p_i}. \tag{13}$$

Eq. 1 and Eq. 13 can be combined to a coupled system of equations, as follows

$$\begin{bmatrix} \mathbf{A} & -\mathbf{C_{sf}} \\ -\omega^2\rho\mathbf{GS^{-1}C_{fs}} & \mathbf{H} \end{bmatrix} \begin{Bmatrix} \mathbf{u} \\ \mathbf{p} \end{Bmatrix} = \begin{Bmatrix} \mathbf{f_s} \\ \mathbf{p_i} \end{Bmatrix}. \tag{14}$$

In fact, direct iterations on the combined equation shown above converge very slowly, and solving directly the system equation will take much more computing time and storage requirement. In addition, it is difficult to obtain the numerical solutions with high accuracy. Instead of solving the above non-symmetric of linear equation using an iterative solver, we propose the following approach. By substituting Eq. 4 into Eq. 13, one can obtain the following coupled boundary element equation

$$\mathbf{Hp} - \mathbf{GWC_{sf}p} = \mathbf{GWf_s} + \mathbf{p_i}, \tag{15}$$

where matrix $\mathbf{W} = \omega^2\rho\mathbf{S^{-1}C_{fs}A^{-1}}$. FMM and the iterative solver GMRES were applied to accelerate the solution of the coupled boundary element system equation. It is worth noting that matrix $\mathbf{A}$ is frequency-dependent. And for solving $\mathbf{A^{-1}}$, an adapted modal reduction method that can be used instead of a direct solution can be found in [Dazel, Sgard, and Lamarque (2003)]. However, in order to obtain the solution of $\mathbf{A^{-1}y}$, in this paper we will use a sparse direct solver to solve the symmetric and frequency-dependent system of linear equation $\mathbf{Ax} = \mathbf{y}$.

3 Shape design sensitivity analysis

The goal of the shape optimization is to find the best design parameters defining the desired shape of the given structure under certain constraints. Shape design sensitivity analysis is a procedure to calculate gradients of cost functions defined. The obtained gradients can then be used to determine the direction to search the optimum values of the design variables. Accordingly, acoustic shape sensitivity analysis is usually the first and most important step in acoustic shape design and optimization processes.

The direct method in the sensitivity formulation is to first calculate the sensitivity of the state variable and then to use the chain rule of differentiation to calculate the sensitivity of the performance function. This method is popular because it is closely related to the analysis procedure.

3.1 Shape design sensitivity analysis based on FEM

First, by differentiating Eq. 1 with respect to the shape design variable, we can obtain the following formulation

$$(\dot{\mathbf{K}}+i\omega\dot{\mathbf{C}}-\omega^2\dot{\mathbf{M}})\mathbf{u}+(\mathbf{K}+i\omega\mathbf{C}-\omega^2\mathbf{M})\dot{\mathbf{u}}=\dot{\mathbf{A}}\mathbf{u}+\mathbf{A}\dot{\mathbf{u}}=\dot{\mathbf{f}}, \tag{16}$$

where the upper dot $\dot{(\ )}$ denotes the differentiation with respect to the design variable. In fact, the expressions of matrices $\dot{\mathbf{K}}$, $\dot{\mathbf{C}}$, $\dot{\mathbf{M}}$ and $\dot{\mathbf{A}}$, can be complicated especially when the structure domain is approximated using shell finite elements. And so it is very difficult to solve them directly. But the semi-analytical derivative method , in which the variation of the coefficient matrices can be calculated using the finite difference method, can be applied to conquer the difficulty. For example, the matrix $\dot{\mathbf{C}}$ can be calculated using a small perturbation τ when the shape design variable is denoted by α, as follows

$$\dot{\mathbf{C}}=\frac{\mathbf{C}(\alpha+\tau)-\mathbf{C}(\alpha)}{\tau}. \tag{17}$$

3.2 Shape design sensitivity analysis based on BEM

By differentiating Eq. 9 with respect to an arbitrary design variable, one can obtain the following formulations for acoustic design sensitivity analysis:

$$\begin{aligned}C(x)\dot{p}(x)=&\int_S[\dot{G}(x,y)q(y)-\dot{F}(x,y)p(y)]dS(y)+\int_S[G(x,y)\dot{q}(y)-F(x,y)\dot{p}(y)]dS(y)\\&+\int_S[G(x,y)q(y)-F(x,y)p(y)]d\dot{S}(y)+\dot{p}_i(x),\end{aligned} \tag{18}$$

where $\dot{G}(x,y)$ and $\dot{F}(x,y)$ can be expressed in the form of the coordinate sensitivity, as follows

$$\dot{G}(x,y) = -\frac{ik}{4}H_1^{(1)}(kr)\dot{r}, \tag{19}$$

$$\dot{F}(x,y) = -\frac{ik}{4}H_1^{(1)}(kr)[\frac{(\dot{y}_j-\dot{x}_j)n_j(y)}{r}+r_{,j}\dot{n}_j(y)] + \frac{ik^2}{4}H_2^{(1)}(kr)\dot{r}r_{,j}n_j(y), \tag{20}$$

where

$$\dot{r} = r_{,j}(\dot{y}_j-\dot{x}_j), \tag{21}$$

$\dot{x}_j$ and $\dot{y}_j$ will be evaluated when the boundary of the analyzed domain is fully parameterized with the shape design variable. According to [Haug, Choi, and Komkov (1986)], $\dot{n}_l(y)$ and $d\dot{S}(y)$ can be written as

$$\dot{n}_l(y) = -\dot{y}_{j,l}n_j(y) + \dot{y}_{j,m}n_j(y)n_m(y)n_l(y), \tag{22}$$

and

$$d\dot{S}(y) = [\dot{y}_{l,l} - \dot{y}_{l,j}n_l(y)n_j(y)]dS(y), \tag{23}$$

where an index after a comma denotes the partial derivative with respect to the coordinate component and $\dot{y}_{j,m} = \partial\dot{y}_j/\partial y_m$.

3.3 Shape design sensitivity analysis for coupled boundary element equation

First, by differentiating Eq. 15 with respect to the shape design variable, we can obtain the following formulation

$$\mathbf{H}\dot{\mathbf{p}} - \mathbf{G}\mathbf{W}\mathbf{C_{sf}}\dot{\mathbf{p}} = \dot{\mathbf{G}}\mathbf{a} + \mathbf{G}\mathbf{b} - \dot{\mathbf{H}}\mathbf{p} + \dot{\mathbf{p}}_\mathbf{i}, \tag{24}$$

where vectors $\mathbf{a}$ and $\mathbf{b}$ are defined by

$$\mathbf{a} = \mathbf{W}\mathbf{C_{sf}}\mathbf{p} + \mathbf{W}\mathbf{f_s}, \tag{25}$$

$$\mathbf{b} = \dot{\mathbf{W}}\mathbf{C_{sf}}\mathbf{p} + \mathbf{W}\dot{\mathbf{C}}_\mathbf{sf}\mathbf{p} + \dot{\mathbf{W}}\mathbf{f_s} + \mathbf{W}\dot{\mathbf{f}}_\mathbf{s}, \tag{26}$$

$$\dot{\mathbf{W}} = \omega^2\rho(\dot{\mathbf{S}}^{-1}\mathbf{C_{fs}}\mathbf{A}^{-1} + \mathbf{S}^{-1}\dot{\mathbf{C}}_\mathbf{fs}\mathbf{A}^{-1} + \mathbf{S}^{-1}\mathbf{C_{fs}}\dot{\mathbf{A}}^{-1}). \tag{27}$$

After obtaining all the unknown boundary acoustic pressure values by solving Eq. 15 and subsequently substituting all the boundary acoustic pressure into Eq. 24, we can get the computational solution of the matrix-vector products on the right hand side of Eq. 24. In fact, the expressions of matrices determining vector $\mathbf{b}$, such as $\dot{\mathbf{S}}^{-1}$, $\dot{\mathbf{C}}_{\mathbf{fs}}$ and $\dot{\mathbf{C}}_{\mathbf{sf}}$, can be complicated especially when the structural domain is approximated using shell finite elements. And so it is very difficult to solve them directly. But the semi-analytical derivative method in Eq. 17 can be applied to conquer the difficulty.

It is worth noting that solving directly the inverse of matrix $\mathbf{A}$ in Eq. 27 will be very expensive and it is very difficult to get the variation of inverse of matrix $\mathbf{A}$ by using directly the finite difference method. But $\dot{\mathbf{A}}^{-1}$can be replaced by the following formulation

$$\dot{\mathbf{A}}^{-1} = \mathbf{A}^{-1}\dot{\mathbf{A}}\mathbf{A}^{-1}. \tag{28}$$

By substituting Eq. 28 into Eq. 27, we can obtain the solution of $\dot{\mathbf{W}}\mathbf{y}$ efficiently by solving $\mathbf{A}\mathbf{x} = \mathbf{y}$. In fact, it needs much computing time to solve directly matrices $\mathbf{H}$, $\mathbf{G}$, $\dot{\mathbf{H}}$ and $\dot{\mathbf{G}}$ in Eq. 24 by using conventional BEM since the matrices are full and un-symmetric. But, fast multipole method and the iterative solver GMRES can be applied to accelerate the matrix-vector products.

4 Fast multipole BEM

4.1 Original FMM formulations for acoustic state analysis

With Graf's addition theorem, the Green's function in Eq. 10 can be expanded into the following series:

$$G(x,y) = \frac{i}{4}\sum_{n=-\infty}^{+\infty} O_n(\overrightarrow{y_c x})I_{-n}(\overrightarrow{y_c y}), \tag{29}$$

where y_c is an expansion point near y, the functions O_n and I_n are defined by

$$O_n(\mathbf{x}) = i^n H_n^{(1)}(kr)e^{in\theta}, \tag{30}$$

and

$$I_n(\mathbf{x}) = (-i)^n J_n(kr)e^{in\theta}, \tag{31}$$

where J_n denotes the n-th order Bessel function, (r,θ) indicates the polar coordinate of vector $\mathbf{x}$.

S_0 stands for a subset of the boundary S, which is far away from the source point x. First, the integrals in Eq. 9 can be reformulated by

$$A_2 = \int_{S_0} [G(x,y)q(y) - F(x,y)p(y)]dS(y). \tag{32}$$

By substituting Eq. 29 into Eq. 32, we can obtain the following formulas:

$$A_2 = \sum_{n=-\infty}^{+\infty} O_n(\overrightarrow{y_c x}) M_n(y_c), \tag{33}$$

where M_n is the multipole moment defined by

$$M_n(y_c) = \frac{i}{4} \int_{S_0} [I_{-n}(\overrightarrow{y_c y}) q(y) - D_n(\overrightarrow{y_c y}) p(y)] dS(y), \tag{34}$$

where y_c is located close to S_0 and $D_n(\overrightarrow{y_c y})$ is given by

$$D_n(\overrightarrow{y_c y}) = \frac{\partial I_{-n}(\overrightarrow{y_c y})}{\partial n(y)}. \tag{35}$$

The M2M, M2L, L2L translation formulas are given by

$$M_n(y_c^1) = \sum_{m=-\infty}^{+\infty} I_{-n+m}(\overrightarrow{y_c^1 y_c}) M_m(y_c), \tag{36}$$

$$L_n(x_l) = \sum_{m=-\infty}^{+\infty} (-1)^n O_{n-m}(\overrightarrow{y_c^1 x_l}) M_{-m}(y_c^1), \tag{37}$$

and

$$L_n(x_l^1) = \sum_{m=-\infty}^{+\infty} I_{n-m}(\overrightarrow{x_l^1 x_l}) L_m(x_l), \tag{38}$$

where y_c^1 is located close to S_0, x_l and x_l^1 close to x, as shown in Fig. 1. To the end, one can obtain the following formulations:

$$A_2 = \sum_{n=-\infty}^{+\infty} I_{-n}(\overrightarrow{x_l^1 x}) L_n(x_l^1). \tag{39}$$

4.2 Diagonal formulations for acoustic state analysis

The plane wave expansion of the Green's function in Eq. 10 can be written as

$$G(x,y) = \frac{i}{8\pi} \oint e^{ik\widehat{k}\cdot\overrightarrow{x_l x}} T(\theta, \overrightarrow{y_c x_l}) e^{-ik\widehat{k}\cdot\overrightarrow{y_c y}} d\theta, \tag{40}$$

where

$$\widehat{k}(\theta) = (\cos\theta, \sin\theta), \tag{41}$$

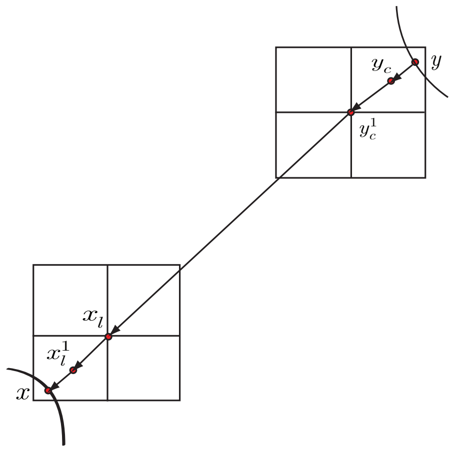

Figure 1: Multipole expansion points and the boundary nodes

and

$$T(\theta,\overrightarrow{y_c x_l}) = \sum_{n=-\infty}^{\infty} e^{-in\theta} O_n(\overrightarrow{y_c x_l}). \tag{42}$$

By substituting Eq. 40 into Eq. 32, one can obtain the following formulation

$$A_2 = \frac{i}{8\pi} \oint e^{ik\hat{k}\cdot\overrightarrow{x_l x}} T(\theta,\overrightarrow{y_c x_l}) B(\theta, y_c) d\theta, \tag{43}$$

where $B(\theta, y_c)$ is the high-frequency moments defined by

$$B(\theta, y_c) = \int_{S_0} [e^{-ik\hat{k}\cdot\overrightarrow{y_c y}} q(y) - E(\overrightarrow{y_c y}) p(y)] dS(y), \tag{44}$$

and

$$E(\overrightarrow{y_c y}) = \frac{\partial e^{-ik\hat{k}\cdot\overrightarrow{y_c y}}}{\partial n(y)}. \tag{45}$$

The B2B, B2H and H2H translation formulas are given by

$$B(\theta, y_c^1) = e^{-ik\hat{k}\cdot\overrightarrow{y_c^1 y_c}} B(\theta, y_c), \tag{46}$$

$$H(\theta,x_l) = T(\theta,\overrightarrow{y_c^1 x_l})B(\theta,y_c^1), \tag{47}$$

and

$$H(\theta,x_l^1) = e^{ik\widehat{k}\cdot\overrightarrow{x_l x_l^1}}H(\theta,x_l). \tag{48}$$

To the end, the boundary integrals can be expressed as

$$A_2 = \frac{i}{8\pi}\oint e^{ik\widehat{k}\cdot\overrightarrow{x_l^1 x}}H(\theta,x_l^1)d\theta. \tag{49}$$

4.3 Original FMM formulations for acoustic design sensitivity analysis

By differentiating Eq. 29 with respect to the design variable, one can obtain the following expression:

$$\dot{G}(x,y) = \frac{i}{4}\sum_{n=-\infty}^{+\infty}\dot{O}_n(\overrightarrow{y_c x})I_{-n}(\overrightarrow{y_c y}) + \frac{i}{4}\sum_{n=-\infty}^{+\infty}O_n(\overrightarrow{y_c x})\dot{I}_{-n}(\overrightarrow{y_c y}), \tag{50}$$

and then, one can obtain

$$\dot{F}(x,y) = \frac{i}{4}\sum_{n=-\infty}^{+\infty}\dot{O}_n(\overrightarrow{y_c x})D_n(\overrightarrow{y_c y}) + \frac{i}{4}\sum_{n=-\infty}^{+\infty}O_n(\overrightarrow{y_c x})\dot{D}_n(\overrightarrow{y_c y}), \tag{51}$$

where $\dot{I}_{-n}(\overrightarrow{y_c y})$ and $\dot{D}_n(\overrightarrow{y_c y})$ are defined by

$$\dot{I}_{-n}(\overrightarrow{y_c y}) = (-i)^n[nJ_n(kr)(\frac{\dot{r}}{r} - i\dot{\theta}) - J_{n+1}(kr)k\dot{r}]e^{-in\theta}, \tag{52}$$

and

$$\begin{aligned}\dot{D}_n(\overrightarrow{y_c y}) =& (-i)^n e^{-i(\beta+n\theta)} \times \{J_{n-1}(kr)[\frac{\dot{r}(n-1)}{r} - i(\dot{\beta}+n\dot{\theta})] - k\dot{r}J_n(kr)\} \\ & - (-i)^n e^{i(\beta-n\theta)} \times \{J_{n+1}(kr)[\frac{\dot{r}(n+1)}{r} + i(\dot{\beta}-n\dot{\theta})] - k\dot{r}J_{n+2}(kr)\},\end{aligned} \tag{53}$$

where β denotes the angle between the vector from y_c to y and the outward normal at point y. First, the integrals in Eq. 18 can be reformulated by:

$$D_1 = \int_{S_0}[\dot{G}(x,y)q(y) - \dot{F}(x,y)p(y)]dS(y), \tag{54}$$

$$D_2 = \int_{S_0}[G(x,y)\dot{q}(y) - F(x,y)\dot{p}(y)]dS(y), \tag{55}$$

and

$$D_3 = \int_{S_0} [G(x,y)q(y) - F(x,y)p(y)]d\dot{S}(y). \tag{56}$$

Then, by substituting Eqs. 29, 50 and 51 into Eqs. 54-56, one can obtain the following formulations:

$$D_1 = \sum_{n=-\infty}^{\infty} \dot{O}_n(\overrightarrow{y_c x})M_n(y_c) + \sum_{n=-\infty}^{\infty} O_n(\overrightarrow{y_c x})M_n^1(y_c), \tag{57}$$

$$D_2 = \sum_{n=-\infty}^{\infty} O_n(\overrightarrow{y_c x})M_n^2(y_c), \tag{58}$$

and

$$D_3 = \sum_{n=-\infty}^{\infty} O_n(\overrightarrow{y_c x})M_n^3(y_c), \tag{59}$$

where

$$M_n^1(y_c) = \frac{i}{4}\int_{S_0} [\dot{I}_{-n}(\overrightarrow{y_c y})q(y) - \dot{D}_n(\overrightarrow{y_c y})p(y)]dS(y), \tag{60}$$

$$M_n^2(y_c) = \frac{i}{4}\int_{S_0} [I_{-n}(\overrightarrow{y_c y})\dot{q}(y) - D_n(\overrightarrow{y_c y})\dot{p}(y)]dS(y), \tag{61}$$

and

$$M_n^3(y_c) = \frac{i}{4}\int_{S_0} [I_{-n}(\overrightarrow{y_c y})q(y) - D_n(\overrightarrow{y_c y})p(y)]d\dot{S}(y). \tag{62}$$

Actually, the M2M, M2L, L2L translation formulas for Eqs. 60-62 are the same as Eqs. 36-38. Finally D_1, D_2 and D_3 can be expressed in terms of local expansion coefficients as

$$D_1 = \sum_{n=-\infty}^{\infty} \dot{I}_{-n}(\overrightarrow{x_l x})L_n(x_l) + \sum_{n=-\infty}^{\infty} I_{-n}(\overrightarrow{x_l x})L_n^1(x_l), \tag{63}$$

$$D_2 = \sum_{n=-\infty}^{\infty} I_{-n}(\overrightarrow{x_l x})L_n^2(x_l), \tag{64}$$

and

$$D_3 = \sum_{n=-\infty}^{\infty} I_{-n}(\overrightarrow{x_l x})L_n^3(x_l). \tag{65}$$

4.4 Diagonal formulations for acoustic sensitivity analysis

By differentiating Eq. 40 with respect to the design variable, one can obtain the following expression:

$$\dot{G}(x,y) = \frac{i}{8\pi}\oint e^{ik\dot{\hat{k}}\cdot\overrightarrow{x_l x}}T(\theta,\overrightarrow{y_c x_l})e^{-ik\hat{k}\cdot\overrightarrow{y_c y}}d\theta + \frac{i}{8\pi}\oint e^{ik\hat{k}\cdot\overrightarrow{x_l x}}T(\theta,\overrightarrow{y_c x_l})e^{-ik\dot{\hat{k}}\cdot\overrightarrow{y_c y}}d\theta, \tag{66}$$

and then, one can obtain

$$\dot{F}(x,y) = \frac{i}{8\pi}\oint e^{ik\dot{\hat{k}}\cdot\overrightarrow{x_l x}}T(\theta,\overrightarrow{y_c x_l})E(\theta,\overrightarrow{y_c y})d\theta + \frac{i}{8\pi}\oint e^{ik\hat{k}\cdot\overrightarrow{x_l x}}T(\theta,\overrightarrow{y_c x_l})\dot{E}(\theta,\overrightarrow{y_c y})d\theta. \tag{67}$$

By substituting Eqs. 66 and 67 into Eqs. 54-56, one can obtain the following formulations:

$$D_1 = \frac{i}{8\pi}\oint e^{ik\dot{\hat{k}}\cdot\overrightarrow{x_l x}}T(\theta,\overrightarrow{y_c x_l})B(\theta,y_c)d\theta + \frac{i}{8\pi}\oint e^{ik\hat{k}\cdot\overrightarrow{x_l x}}T(\theta,\overrightarrow{y_c x_l})B^1(\theta,y_c)d\theta, \tag{68}$$

$$D_2 = \frac{i}{8\pi}\oint e^{ik\hat{k}\cdot\overrightarrow{x_l x}}T(\theta,\overrightarrow{y_c x_l})B^2(\theta,y_c)d\theta, \tag{69}$$

and

$$D_3 = \frac{i}{8\pi}\oint e^{ik\hat{k}\cdot\overrightarrow{x_l x}}T(\theta,\overrightarrow{y_c x_l})B^3(\theta,y_c)d\theta, \tag{70}$$

where

$$B^1(\theta,y_c) = \int_{S_0}[e^{-ik\dot{\hat{k}}\cdot\overrightarrow{y_c y}}q(y) - \dot{E}(\theta,\overrightarrow{y_c y})p(y)]dS(y), \tag{71}$$

$$B^2(\theta,y_c) = \int_{S_0}[e^{-ik\hat{k}\cdot\overrightarrow{y_c y}}\dot{q}(y) - E(\theta,\overrightarrow{y_c y})\dot{p}(y)]dS(y), \tag{72}$$

and

$$B^3(\theta,y_c) = \int_{S_0}[e^{-ik\hat{k}\cdot\overrightarrow{y_c y}}q(y) - E(\theta,\overrightarrow{y_c y})p(y)]d\dot{S}(y). \tag{73}$$

Actually, the B2B, B2H and H2H translation formulas for Eqs. 71-73 are the same as Eqs. 46-48. Finally D_1, D_2 and D_3 can be expressed in terms of local expansion coefficients as

$$D_1 = \frac{i}{8\pi}\oint e^{ik\dot{\hat{k}}\cdot\overrightarrow{x_l x}}H(\theta,x_l)d\theta + \frac{i}{8\pi}\oint e^{ik\hat{k}\cdot\overrightarrow{x_l x}}H^1(\theta,x_l)d\theta, \tag{74}$$

$$D_2 = \frac{i}{8\pi} \oint e^{ik\widehat{k}\cdot\overrightarrow{x_l x}} H^2(\theta, x_l) d\theta, \tag{75}$$

and

$$D_3 = \frac{i}{8\pi} \oint e^{ik\widehat{k}\cdot\overrightarrow{x_l x}} H^3(\theta, x_l) d\theta. \tag{76}$$

4.5 Wideband FMM formulations

The wideband FMBEM obtained by combining the original form and the diagonal form of the FMBEM is accurate and efficient at any frequency. In the wideband FMBEM, we use the following M2B formula to convert the moments of the original form to those of the diagonal form:

$$B(\theta, y_c) = -4i \sum_{n=-\infty}^{+\infty} e^{in\theta} M_n(y_c). \tag{77}$$

The local expansion coefficients of the diagonal form can be converted to those of the original form by using the following H2L formula:

$$L_n(x_l) = \frac{i}{8\pi}(-1)^n \oint e^{in\theta} H(\theta, x_l) d\theta. \tag{78}$$

Actually, the number of terms used in the functions O, I, M and L and the number of the plane wave samples $\widehat{k}$ along the unit circle have to be truncated. The number of truncation terms and the plane wave samples depends on the size d of the cell and the wave number k. It is given in the following form in [Coifman, Rokhlin, and Wandzura (1993)]:

$$p = kd + c \cdot \log(kd + \pi). \tag{79}$$

where c is a constant. Obviously, a larger c relates to a larger truncation number p and it normally leads to an improvement of accuracy but induces to a longer computing time and larger memory usage. Thus, it is a key parameter in the FMM algorithm, which is chosen as 5 in this paper based on our previous research [Chen, Zheng, and Chen (2013)].

5 Numerical examples

5.1 Scattering from an infinite rigid cylindrical shell

A numerical simulation of acoustic scattering from an infinite rigid cylindrical shell with Neumann boundary condition is given to demonstrate the accuracy and efficiency of the present algorithm. The computation is done on a desktop PC with an Pentium 2.59 GHz processor and 3.24 GB memory.

In this example, we consider the acoustic scattering of a plane incident wave with unit amplitude on an infinite rigid cylindrical shell with radius $a = 1.0$m centred at point $(0,0)$, and the plane incident wave is travelling along the positive x axis ($\theta = 0$), as shown in Fig. 2. The analytical solution of the sound pressure at point (r,θ) is given as

$$p(r,\theta) = -\sum_{n=0}^{\infty} \varepsilon_n i^n \frac{J_n'(ka)}{H_n^{(1)\prime}(ka)} H_n^{(1)}(kr)\cos(n\theta), \tag{80}$$

where ε_n denotes the Neumann symbols, i.e., $\varepsilon_0 = 1$; $\varepsilon_n = 2$ when n is greater than 0. $(\ )'$ stands for the differentiation with respect to ka.

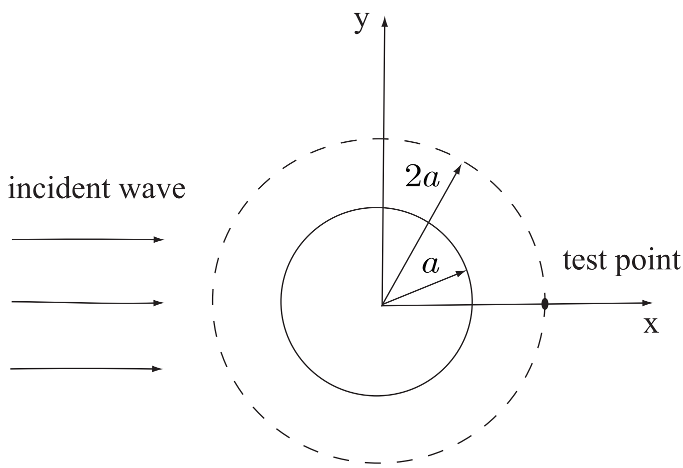

Figure 2: Scattering from an infinite cylindrical shell with radius a

When the design variable is chosen as a, one can obtain the analytical solution of sound pressure sensitivity by differentiating Eq. 80 with respect to the design variable, as follows:

$$\frac{\partial p(r,\theta)}{\partial a} = -\sum_{n=0}^{\infty} \varepsilon_n i^n \left[\frac{J_n'(ka)}{H_n^{(1)\prime}(ka)}\right]' H_n^{(1)}(kr)\cos(n\theta). \tag{81}$$

Sample internal points are evenly distributed on a circle of $r = 2a$ and the coordinates of the test point are $(2a,0)$. The boundary of the circle is discretized with 80000 constant elements and the maximum number of boundary elements in per leaf is set to 60. With this parameter, the number of tree levels in the tree structure is 10, the number of leaves is 2196 and the number of cells is 3829.

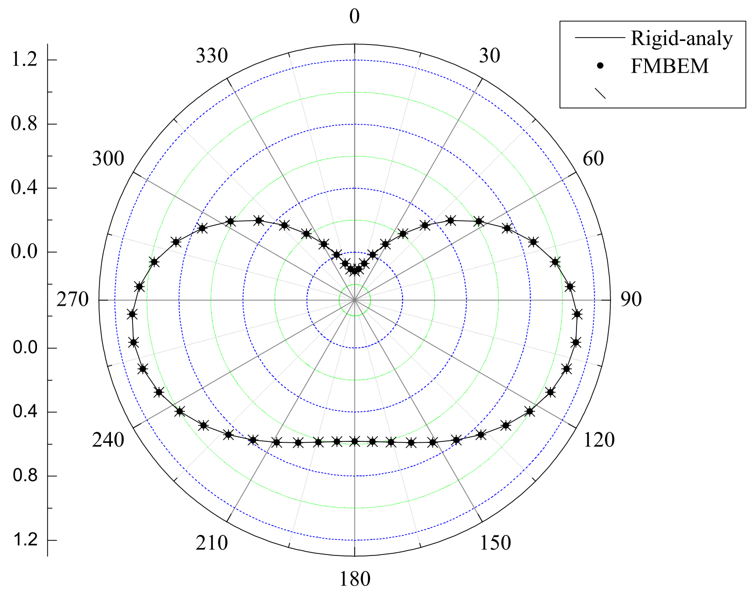

Figure 3: Real part of pressure at points on circle $r = 2a$ with $k = 2$

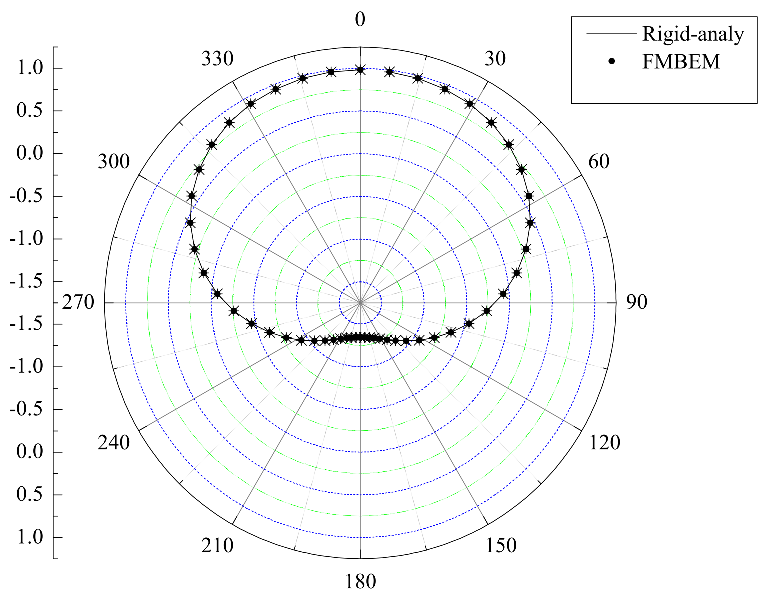

Figure 4: Imaginary part of pressure at points on circle $r = 2a$ with $k = 2$

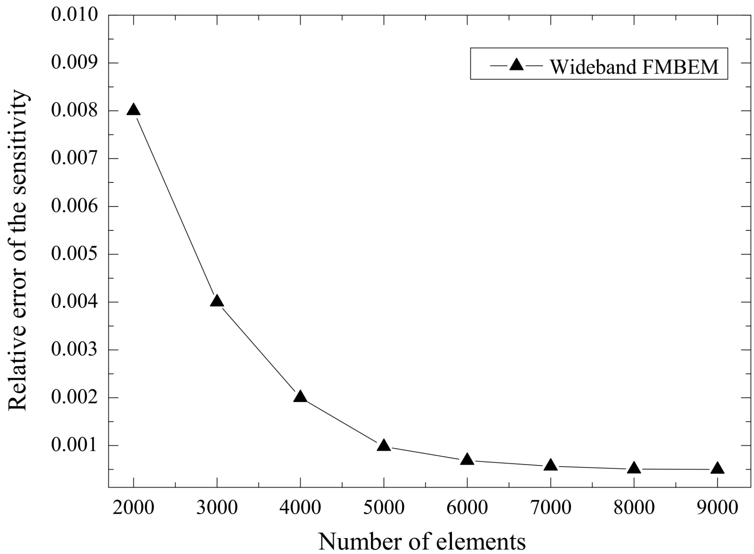

Figure 5: Relative error of the pressure sensitivity at point $(2a,0)$ with $k=4\pi$

From Figs. 3 and 4, it can be seen that numerical result obtained by using FMBEM and CBEM both agree very well with the analytical solution which is denoted by the symble "Rigid-analy", and it demonstrates the accuracy of the algorithm. The relative error is defined as

$$error = \frac{|p_{numer} - p_{analy}|}{|p_{analy}|}, \tag{82}$$

where the p_{numer} denotes the numerical solution and the p_{analy} denotes the analytical solution. Actually, in the numerical evaluation of these boundary integral equations, truncation and numerical integration errors are the main errors. And estimates for these errors can be found in [Amini and Prot (2000)]. Due to the complexity of the differential equations, giving a provement of the uniform convergence of the numerical results is very hard and is not the key point for this work. However, by observing Fig. 5, it can be found that the solution converges well when refining the boundary mesh and it implicates the accuracy of the presented algorithm. The CPU time used to calculate the sensitivity values at the test point is plotted in Fig. 6, which demonstrates the efficiency of FMBEM for two dimensional acoustic design sensitivity analysis.

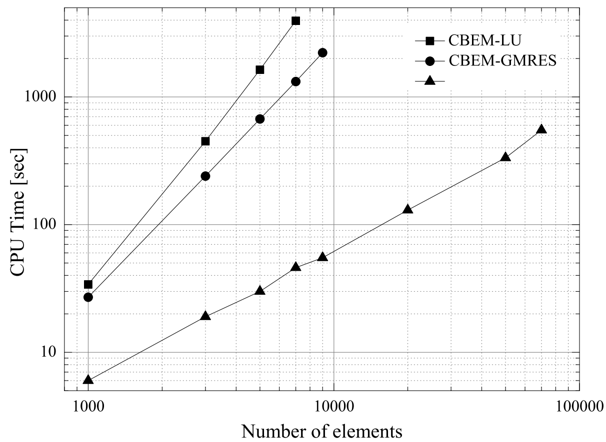

Figure 6: CPU time used to calculate the pressure sensitivity values at point $(2a, 0)$ with $k = 4\pi$

5.2 *Scattering from an infinite elastic cylindrical shell*

In this example, we consider the acoustic scattering of a plane incident wave with unit amplitude on an elastic cylindrical shell with radius $a = 1.0m$ centred at point $(0,0)$, as shown in Fig 2. For the cylindrical shell, the thickness is chosen as $0.01m$, Young's modulus $2 \times 10^{11} Pa$, Poisson's ratio 0.26 and the density $7800 kg/m^3$. For the fluid, the density is chosen as $1000 kg/m^3$ and the speed of sound $1524 m/s$. The benchmark solution to which the numerical results will be compared is the series solution published by Junger and Feit [Junger and Feit (1985)].

In Figs. 7 and 8, "FEM/WFMBEM" denotes numerical solution obtained by using coupling FEM and wideband FMBEM, and "Ela-analy" denotes analytical solution. From the two figures, it can be seen that numerical results obtained by using FEM/BEM and FEM/WFMBEM both agree very well with the analytical solutions at the sample internal points, and it demonstrates the accuracy of the presented algorithm. Figures 9 and 10 show a low-frequency comparison between the acoustic pressure values based on the rigid scattering and the elastic scattering, and it denotes that the fluid has a big impact on the vibrating and scattering acoustic field from the underwater thin shell structure. From the two figures, it can also be seen that the numerical results obtained by using FEM/BEM and FEM/FMBEM both agree very well with the analytical solutions at the test point. The CPU time used to calculate the acoustic pressure values is plotted in Fig. 11, which demonstrates the

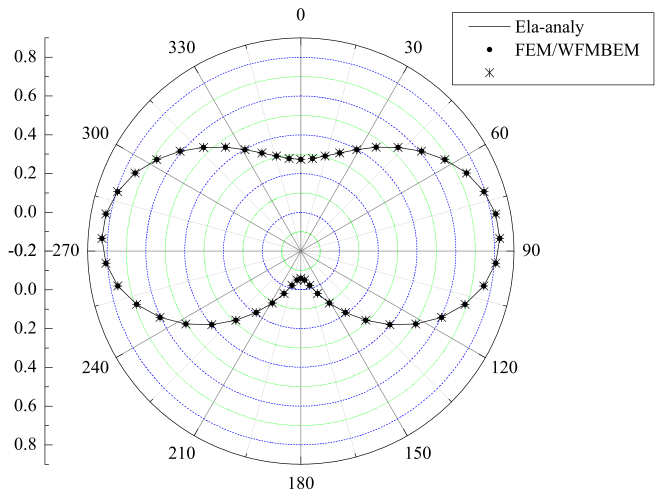

Figure 7: Real part of acoustic pressure at points on circle $r = 2a$ with $k = 2$

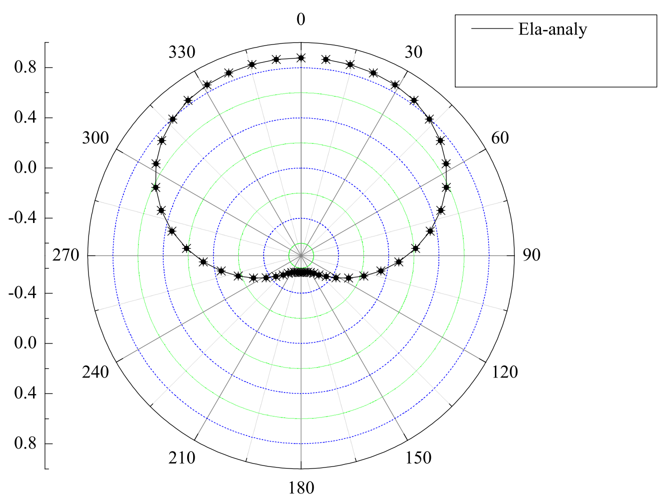

Figure 8: Imaginary part of acoustic pressure at points on circle $r = 2a$ with $k = 2$

high efficiency of FEM/Wideband FMBEM algorithm for two dimensional fluid-structure interaction problems. Figures 12 and 13 show that the acoustic pressure sensitivity values obtained by using FEM/Wideband FMBEM algorithm agree well with the analytical solutions at the test point and it implicates the accuracy of the presented algorithm, where the design variable is chosen as the radius a of the cylindrical shell.

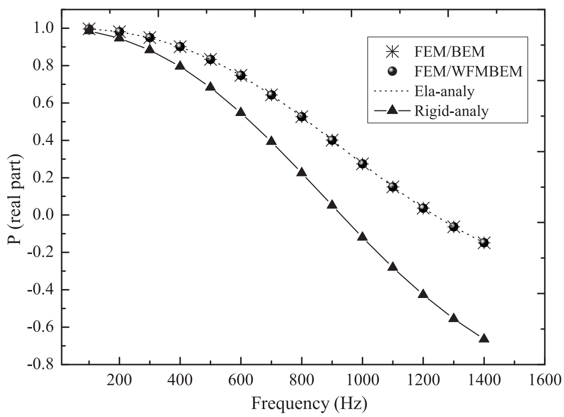

Figure 9: Real part of acoustic pressure at the test point with different frequencies

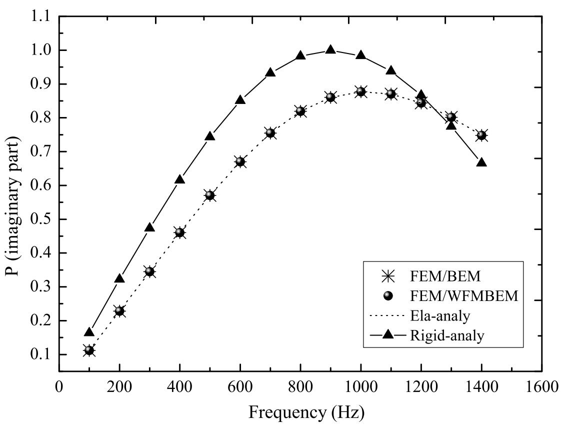

Figure 10: Imaginary part of acoustic pressure at the test point with different frequencies

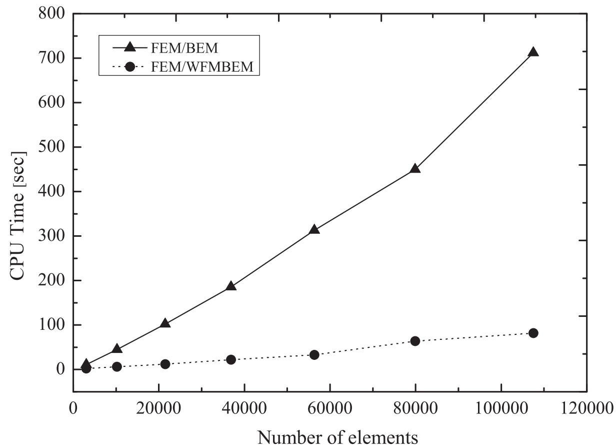

Figure 11: CPU time used to calculate the acoustic pressure at the test point with $k = 2$

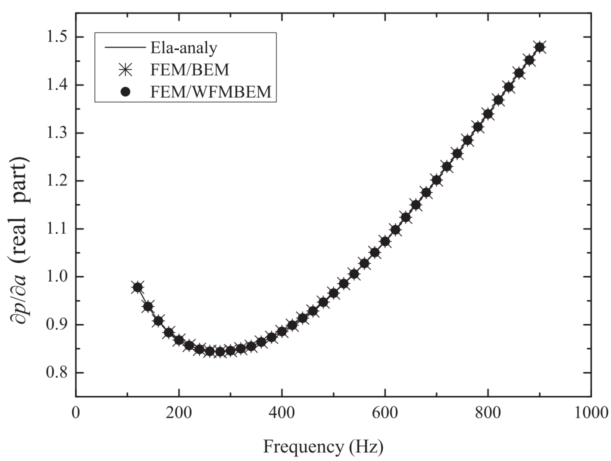

Figure 12: Real part of acoustic pressure sensitivity at the test point with different frequencies

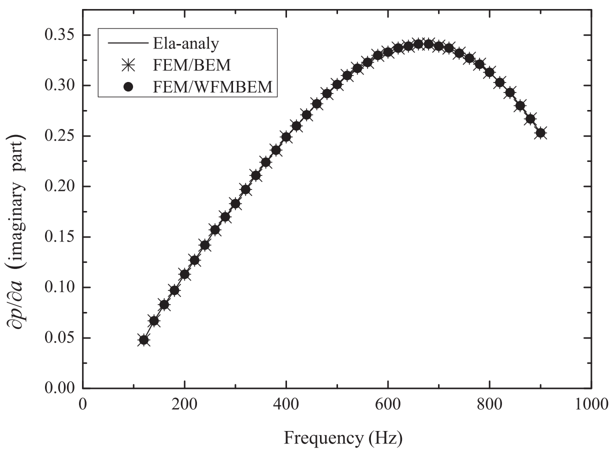

Figure 13: Imaginary part of acoustic pressure sensitivity at the test point with different frequencies

6 Conclusions

A coupling algorithm based on FEM and wideband FMBEM is presented for the simulation of fluid-structure interaction and structural acoustic sensitivity analysis using the direct differentiation method. The FEM was used to model the structural parts of the problem. To avoid the need to mesh the fluid domain, the wideband FMBEM formed by combining the original FMBEM and the diagonal form FMBEM is used to accelerate the matrix-vector products in the boundary element analysis. The presented algorithm makes it possible to predict the effects of arbitrarily shaped vibrating structures on the sound field numerically.

However, the iterative solution of the system of linear equation based on GMRES method is often the most time-consuming part of the simulation for modeling fluid-structure interaction problems numerically by using the coupling FEM/wideband FMBEM algorithm. The development of a more suitable preconditioner is required and this problem is now being addressed in an ongoing research project. Future work also includes applying the acoustic design sensitivity analysis to shape optimizations and extending the method to three dimensional practical problems.

Acknowledgement: Financial supports from the China Scholarship Council (CSC), the National Natural Science Foundation of China (NSFC) under Grant no. 11172291, China Postdoctoral Science Foundation under Grant no. 2012M510162 and the Fundamental Research Funds for the Central Universities (KB2090050024) are acknowledged.

References

Amini, S.; Prot, A. (2000): Analysis of the truncation errors in the fast multipole method for scattering problems. *J. Comput. Appl. Math.*, vol. 115, pp. 23–33.

Burton, A.; Miller, G. (1971): The application of integral equation methods to the numerical solution of some exterior boundary-value problems . *Proc. Roy. Soc. Lond. A.*, vol. 323, pp. 201–210.

Chen, L.; Zheng, C.; Chen, H. (2013): A wideband FMBEM for 2D acoustic design sensitivity analysis based on direct differentiation method . *Comput. Mech.*, vol. 52, pp. 631–648.

Chen, Z.; Hofstetter, G.; Mang, H. (1998): A Galerkin-type BE-FE formulation for elasto-acoustic coupling. *Comput. Method. Appl. M.*, vol. 152, pp. 147–155.

Cheng, H.; Crutchfield, W.; Gimbutas, Z.; Greengard, L.; Ethridge, J.; Huang, J.; Rokhlin, V.; Yarvin, N.; Zhao, J. (2006): A wideband fast multipole method for the Helmholtz equation in three dimensions . *J. Comput. Phys.*, vol. 216, pp. 300–325.

Coifman, R.; Rokhlin, V.; Wandzura, S. (1993): The fast multipole method for the wave equation: A pedestrian prescription. *IEEE Antennas Propag. Mag.*, vol. 35, pp. 7–12.

Darve, E.; P.Havé (2004): A fast multipole method for Maxwell equations stable at all frequencies. *Phil. Trans. R. Soc. Lond. A.*, vol. 362, pp. 603–628.

Dazel, O.; Sgard, F.; Lamarque, C. (2003): Application of generalized complex modes to the calculation of the forced response of three-dimensional poroelastic materials. *J. Sound. Vib.*, vol. 268, pp. 555–580.

Everstine, G.; Henderson, F. (1990): Coupled finite element/boundary element approach for fluid-structure interaction. *J. Acoust. Soc. Am.*, vol. 87, pp. 1938–1947.

Fischer, M.; Gaul, L. (2005): Fast BEM-FEM mortar coupling for acoustic-structure interaction . *Int. J. Numr. Meth. Eng.*, vol. 62, pp. 1677–1690.

Fritze, D.; Marburg, S.; Hardtke, H. (2005): FEM-BEM-coupling and structural-acoustic sensitivity analysis for shell geometries. *Computers and Structures*, vol. 82, pp. 143–154.

Greengard, L.; Rokhlin, V. (1987): A fast algorithm for particle simulations. *J. Comput. Phys.*, vol. 73, pp. 325–348.

Gumerov, N.; Duraiswami, R. (2009): A broadband fast multipole accelerated boundary element method for the three dimensional Helmholtz equation . *J. Acoust. Soc. Am.*, vol. 125, pp. 191–205.

Haug, E.; Choi, K.; Komkov, V. (1986): *Design sensitivity analysis of structural systems*. Academic Press Inc.

Junger, M. C.; Feit, D. (1985): *Structures and Their Interaction*. MIT Press.

Kim, N.; Dong, J. (2006): Shape sensitivity analysis of seuential structural-acoustic problems using FEM and BEM, Journal of sound and vibration . *Eng. Anal. Boundary Elem.*, vol. 36, pp. 192–208.

Matsumoto, T.; Yamada, T.; Takahashi, T.; Zheng, C.; Harada, S. (2011): Acoustic design shape and topology sensitivity formulations based on adjoint method and BEM. *CMES: Computer Modeling in Engineering & Sciences*, vol. 78, no. 2, pp. 77–94.

Rokhlin, V. (1993): Diagonal forms of translatioin operators for the Helmholtz equation in three dimensions. *Appl. Comput. Harmon. Anal.*, vol. 1, pp. 82–93.

Schneider, S. (2008): FE/FMBE coupling to model fluid-structure interaction . *Int. J. Numr. Meth. Eng.*, vol. 76, pp. 2137–2156.

Shen, L.; Liu, Y. (2007): An adaptive fast multipole boundary element method for three-dimensional acoustic wave problems based on the Burton-Miller formulations. *Comput. Mech.*, vol. 40, pp. 461–472.

Song, J.; Lu, C.; Chew, W. (1997): Multilevel fast multipole algorithm for electromagnetic scattering by large complex objects. *IEEE Trans. Antennas Propag.*, vol. 45, pp. 1488–1493.

Wolf, W.; Lele, S. (2011): Wideband fast multipole boundary element method: Application to acoustic scattering from aerodynamic bodies . *Int. J. Numer. Meth. Fl.*, vol. 67, pp. 2108–2129.

Zheng, C.; Chen, H.; Matsumoto, T.; Takahashi, T. (2011): Three dimensional acoustic shape sensitivity analysis by means of adjoint variable method and fast multipole boundary element approach. *CMES: Computer Modeling in Engineering & Sciences*, vol. 79, no. 1, pp. 1–30.

Zheng, C.; Chen, H.; Matsumoto, T.; Takahashi, T. (2012): 3D acoustic shape sensitivity analysis using fast multipole boundary element method. *Int. J. Comput. Methods.*, vol. 9, pp. 1240004–1–1240004–11.

Zheng, C.; Matsumoto, T.; Takahashi, T.; Chen, H. (2011): Explicit evaluation of hypersingular boundary integral equations for acoustic sensitivity analysis based on direct differentiation method . *Eng. Anal. Boundary Elem.*, vol. 35, pp. 1225–1235.

Zheng, C.; Matsumoto, T.; Takahashi, T.; Chen, H. (2012): A wideband fast multipole boundary element method for three dimensional acoustic shape sensitivity analysis based on direct differentiation method . *Eng. Anal. Boundary Elem.*, vol. 36, pp. 361–371.